CellPress

Cell

Article

RNA polymerase III is required for the repair of DNA double-strand breaks by homologous recombination

Sijie Liu,[1,2] Yu Hua,[1,2] Jingna Wang,[1,2] Lingyan Li,[1,2] Junjie Yuan,[1] Bo Zhang,[1] Ziyang Wang,[1] Jianguo Ji,[1] and Daochun Kong[1,3,*]

[1]Peking-Tsinghua Center for Life Sciences, The National Laboratory of Protein and Plant Gene research, College of Life Sciences, Peking University, Beijing 100871, China

[2]These authors contributed equally

[3]Lead contact

*Correspondence: kongdc@pku.edu.cn

https://doi.org/10.1016/j.cell.2021.01.048

SUMMARY

End resection in homologous recombination (HR) and HR-mediated repair of DNA double-strand breaks (DSBs) removes several kilobases from 5′ strands of DSBs, but 3′ strands are exempted from degradation. The mechanism by which the 3′ overhangs are protected has not been determined. Here, we established that the protection of 3′ overhangs is achieved through the transient formation of RNA-DNA hybrids. The DNA strand in the hybrids is the 3′ ssDNA overhang, while the RNA strand is newly synthesized. RNA polymerase III (RNAPIII) is responsible for synthesizing the RNA strand. Furthermore, RNAPIII is actively recruited to DSBs by the MRN complex. CtIP and MRN nuclease activity is required for initiating the RNAPIII-mediated RNA synthesis at DSBs. A reduced level of RNAPIII suppressed HR, and genetic loss > 30 bp increased at DSBs. Thus, RNAPIII is an essential HR factor, and the RNA-DNA hybrid is an essential repair intermediate for protecting the 3′ overhangs in DSB repair.

INTRODUCTION

Homologous recombination (HR), a universal biological process (Lin et al., 2006; Persky and Lovett, 2008), plays a crucial role in cell division, generation of gamete cells, genetic diversity, and repair of DNA double-strand breaks (DSBs) (Jasin and Rothstein, 2013; Keeney et al., 1997; Marcon and Moens, 2005; Mehta and Haber, 2014; Szostak et al., 1983; Thompson and Schild, 2001; Zhao et al., 2017). HR predominantly occurs in the S and G2 phases of the cell cycle, as sister chromatids in these phases are available to serve as repair templates. The process of HR and the HR-mediated repair of DSBs consist of three main steps, namely, end resection, strand invasion, and resolution of Holliday junctions (Haber et al., 2004; Orr-Weaver and Szostak, 1983; Rothstein, 1983; Szostak et al., 1983). At the end-resection step, several hundred to several thousand bases are removed from the 5′-ended strand, which generates a 3′ single-stranded DNA (ssDNA) overhang of hundreds to thousands of nucleotides. This 3′ ssDNA overhang then invades a sister chromatid or a neighboring complementary DNA molecule for subsequent HR processes (Daley et al., 2015; Zhang et al., 2016). The nucleases that directly participate in end resection are the CtIP-MRN (MRE11, RAD50, and NBS1) complex, DNA2 flap endonuclease, and EXO1 dsDNA exonuclease, as we know at present (Cannavo and Cejka, 2014; Mimitou and Symington, 2008; Zhang et al., 2016; Zhu et al., 2008). The MRN complex (MRX in budding yeast, MRE11-RAD50-XRS2) has both endonuclease and 3′-5′ exonuclease activities (Deshpande et al., 2016; Paull and Gellert, 1998). The initiation of end resection is carried out by the CtIP-MRN (or SAE2-MRX in budding yeast) complex, which removes approximately a few dozen nucleotides from the 5′-strand end (Cannavo and Cejka, 2014). Besides these nucleases, Sgs1 helicase in budding yeast is also involved in the resection process, because Sgs1 and Dna2 form a complex in budding yeast, and it is demonstrated that Sgs1 is responsible for unwinding the DNA to generate flap structures for Dna2 cleavage (Cejka et al., 2010; Mimitou and Symington, 2008; Niu et al., 2010; Zhu et al., 2008).

In contrast to Sgs1 in budding yeast, Rqh1, the homolog of Sgs1 in the fission yeast *Schizosaccharomyces pombe*, plays only a minor role in end resection, although it was also reported that, in a specific situation, Rqh1 functions for long-range end resection in the absence of Crb2 and Rev7 (Leland et al., 2018). We found that end resection up to 9.4 kb is not much affected in the *rqh1*Δ cells (Zhang et al., 2016), which is consistent with a previous study (Langerak et al., 2011). However, as in budding yeast, Dna2 and Exo1 are required for end resection in *S. pombe* (Zhang et al., 2016). Since *S. pombe* Dna2 has only a modest helicase activity (Hu et al., 2012), this raises the question of how flap structures, a preferred Dna2 substrate, are generated

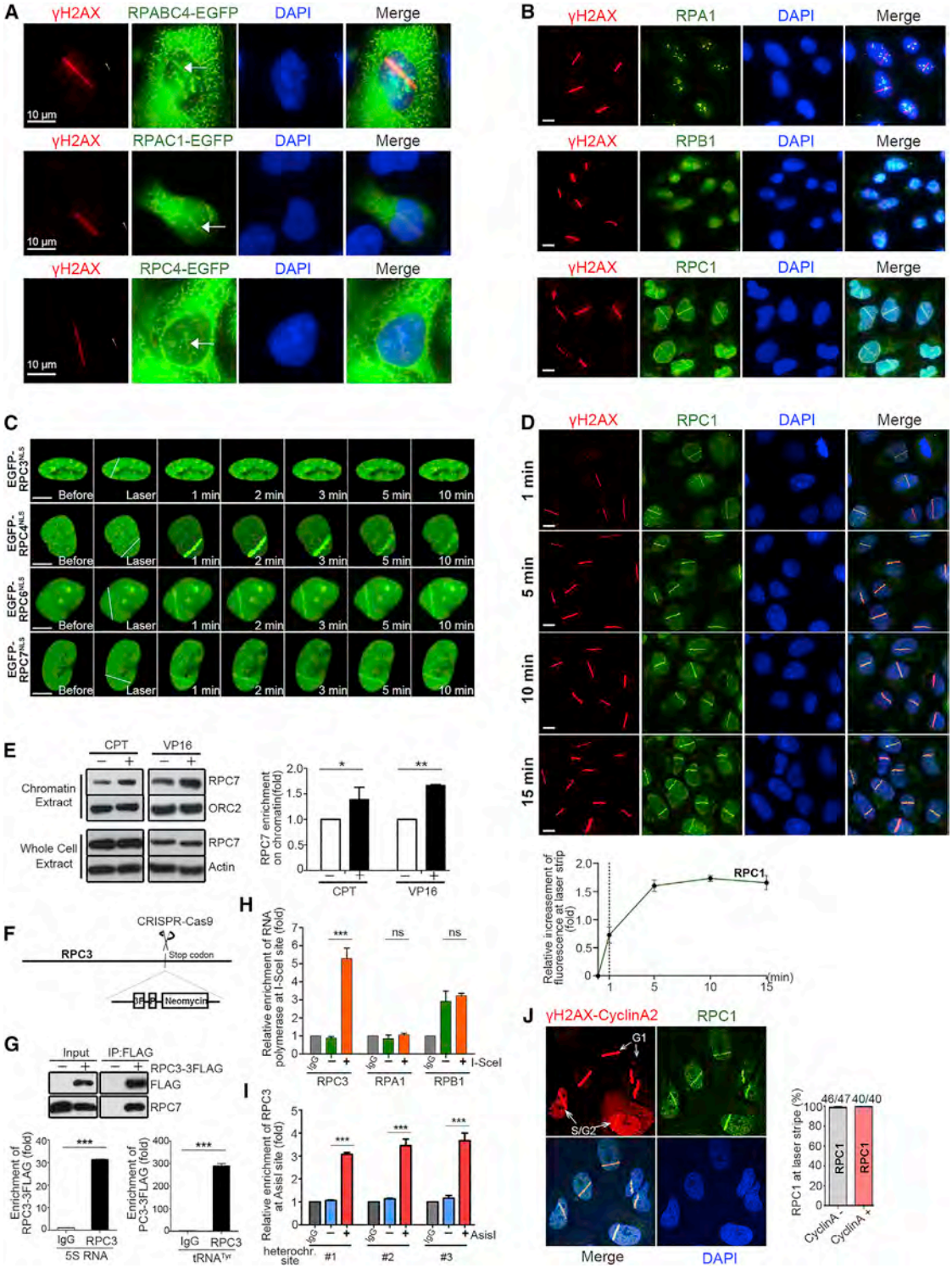

Figure 1. RNA polymerase III localizes to DSBs

The cells used in this experiment were U2OS.

(A) Localization of RPABC4, RPAC1, and RPC4 subunits to DSBs. The log-phase cells were irradiated with a 365-nm laser. Cells were fixed with paraformaldehyde for 5–10 min after laser irradiation. γH2AX was detected by immunostaining with its specific antibody. The RPABC4, RPAC1, and RPC4 subunits were detected by tagged EGFP.

(legend continued on next page)

for end resection in fission yeast. It is possible that *S. pombe* cells may use another helicase for generating flap structures. It is equally possible that another mechanism exists in fission yeast cells to create flap structures. In metazoan or human cells, both *in vitro* and *in vivo* assays show that DNA2 and EXO1 are involved in long-range end resection at DSBs (Nimonkar et al., 2011; Sturzenegger et al., 2014). However, the helicase that functions in end resection remains a matter of debate. There are five homologs of Sgs1 helicase—WRN, RECQ4, BLM, RECQL, and RECQ5β (Hickson, 2003). Studies in *Xenopus* egg extracts showed that Dna2 together with WRN rather than BLM mediates DNA end resection (Liao et al., 2008; Yan et al., 2005). However, an *in vitro* biochemical analysis suggested that BLM, together with DNA2 and EXO1, constitutes two DNA end-resection machineries for DSB repair in human cells (Nimonkar et al., 2011). Thus, the discrepancies in the functional assays of WRN and BLM indicate that the question of whether WRN or BLM function for end resection *in vivo* remains open.

After end resection on the 5′ strands, 3′-ssDNA overhangs are created at DSBs. RAD51 assembles onto the 3′-ssDNA overhang to form a RAD51 nucleoprotein filament. This filament then invades a homologous sequence for subsequent HR or DSB repair processes (San Filippo et al., 2008). Although much is known about the process of end resection, some critical questions still remain to be answered. Among them, the most important one is how the integrity of the 3′-ssDNA overhang is preserved during end resection. A strict protection of the 3′-ssDNA overhang is critical during the extensive resection of the 5′-ended strand(s), as an entire or even a partial removal of the 3′-ssDNA overhang will inhibit HR and potentially results in genetic loss.

Three recent studies reported the observation of RNA-DNA hybrids at DSBs (Li et al., 2016; Michelini et al., 2017; Ohle et al., 2016). Small RNA molecules complementary to the neighboring DNA sequences of DSBs have also been detected (Francia et al., 2012; Wei et al., 2012). Furthermore, it has also been reported that DDX1 RNA helicase, as well as RNase H1/2 and noncoding RNA (ncRNA)-processing RNases, are required for efficient DSB repair by HR and may be involved in removing the RNA strands at DSBs (Francia et al., 2012; Li et al., 2016; Ohle et al., 2016; Wei et al., 2012). However, regarding the RNA-DNA hybrids at DSBs, several critical questions remain, as remarked by Aguilera and Gómez-Gonzalez (2017) and Plosky (2016). First, is the RNA strand at DSB just a transcript at actively transcribed region where DSB happens to occur? Second, is the RNA-DNA hybrid a repair intermediate? Third, if the RNA-DNA hybrid at DSB is actively created, which RNA polymerase is responsible for catalyzing the RNA strand synthesis? Fourth, what is the biological function of the RNA-DNA hybrids in the repair of DSBs?

In this study, we found that RNA polymerase III (RNAPIII) is an essential factor in the HR-mediated repair of DSBs. Moreover, we showed that the formation of RNA-DNA hybrids is an active process and the RNA-DNA hybrid is a repair intermediate in the process of HR and the HR-mediated repair of DSBs. The RNA strand in the hybrids is catalyzed by RNAPIII, and the DNA strand is the 3′-ssDNA overhang. The formation of RNA-DNA hybrids is one of the earliest events in the HR-mediated repair of DSBs. When the formation of the RNA-DNA hybrid was inhibited by either the RNAi-mediated reduction of RNAPIII or a specific chemical inhibitor, it significantly decreased the rate of HR and caused the genetic loss at DSBs, suggesting that the formation of RNA-DNA hybrids protects the 3′-ssDNA overhangs. We further demonstrated that the RNAPIII-mediated RNA synthesis plays an important role in long-range end resection, suggesting that at least some of the flap structures or the displacement of the 5′-strand results from the RNA synthesis. Furthermore, it was found that RNAPIII is actively recruited to DSBs by the MRN complex.

RESULTS

RNA polymerase III localizes to DSB site

To further understand the mechanism of HR and HR-mediated DSB repair, we undertook the search for additional HR factors.

(B) RPC1, but not RPA1 and RPB1, was localized to DSBs. The assay was performed as in (A). After laser irradiation, cells were stained with antibodies against γH2AX, RPA1, RPB1, or RPC1.

(C) RPC3, 4, 6, and 7 were localized to DSBs. These subunits were tagged by an SV40 NLS motif and EGFP at their C terminus and N terminus, respectively, to enhance their nuclear localization. The assay was performed as in (A).

(D) RPC1 was localized to DSBs within the first minute after DNA breaks. Cells were fixed at different time point after laser irradiation and stained with antibody against γH2AX or RPC1. Top: fluorescent images; bottom: relative fluorescent enhancement of RPC1 at laser stripe over time.

(E) Accumulation of RPC7 on chromatin of the CPT- or VP16-treated cells. Chromatin was prepared from the untreated cells and cells that were treated with CPT or VP16 for 3 h. Left, the amounts of RPC7, ORC2, and Actin in whole cells or in chromatin were measured by western blotting analysis with a specific antibody against each of these protein subunits. Right, the quantification of RPC7 enrichment on chromatin.

(F) The genome of U2OS DRGFP cells was edited by CRISPR-Cas9 to integrate 3FLAG (3F), P2A (P), and the neomycin resistance gene just before the stop codon of RPC3.

(G) Western blotting analysis confirmed the interaction of RPC3-3FLAG and RPC7 (left) and the enrichment of RPC3 at 5S RNA and $tRNA^{Tyr}$ genes (right two panels).

(H) A ChIP assay showed the enrichment of RPC3 but not RPA1 and RPB1 at the I-SceI break site.

(I) Enrichment of RPC3 at the AsisI sites (#1 [chr1, 69152046-69161997], #2 [chr1, 181068683-181078609], #3 [chr11, 134890863-134900739]) located in compacted/heterochromatin regions.

(J) RPC1 is localized to DSBs at G1, S, and G2 phases of the cell-division cycle. Cells were fixed for 5–10 min after laser irradiation. γH2AX, CyclinA2, and RPC1 were detected with their specific antibody. The right panel shows the percentage of cells showing RPC1 signal at laser stripe, with the number of examined cells indicated.

In general, about two dozen or more cells were examined for each fluorescent analysis. Data are represented as mean ± SD. Statistical analyses were performed with an unpaired two-tailed Student's test. *$p \leq 0.05$; **$p \leq 0.01$; ***$p \leq 0.001$. The scale bar is 10 μm. See also Figure S1.

293T cells were treated with 5 μM VP-16 (etoposide) for 3 h. Chromatin was isolated and treated with Benzonase nuclease. The chromatin fractions containing broken DNA ends and the proteins associated with them were immunoprecipitated with the antibody against MRE11, a subunit of the MRN complex. The analysis of the brought-down proteins by mass spectrometry detected, besides the known HR factors, some subunits of RNA polymerases, such as RPAC1, RPABC1 and 4, and RPC4 (Table S1). In eukaryotes, except in plants, there are three RNA polymerases, namely, RNA polymerase I, II, and III (RNAPI, II, III), which are responsible for the transcription of rRNA, mRNA, tRNA, and some small RNAs, respectively (Cramer et al., 2008). For RNAPI, II, or III, some subunits are commonly used (Cramer et al., 2008) (Table S2). For instance, RPABC4 is the smallest subunits of RNAPII (RPB) and is also shared by the other two DNA-directed RNA polymerases-RNAPI (RPA) and III (RPC). RPAC1 is the largest common subunit used by RNAPI and III, while RPC4 is RNAPIII-specific subunit. To determine whether an RNA polymerase(s) indeed localizes to DSBs, fluorescence assays were conducted. First, RPAC1, RPABC4, and RPC4 subunits detected by MRN immunoprecipitation (IP) were examined. The EGFP-tagged RPAC1, RPABC4, and RPC4 were individually expressed in U2OS cells. As shown in Figure 1A, the EGFP-tagged subunits RPABC4, RPAC1, and RPC4 were localized to DSBs, and their fluorescence signals clearly overlapped with γH2AX (H2AX phosphorylated on serine 139). This result confirms that RPABC4, RPAC1, and RPC4 are indeed localized to DSBs. This result also suggests that an RNA polymerase may actively localize to DSBs. To determine whether all three RNA polymerases or only one of them is localized to DSBs, the presence of RPA1, RPB1, and RPC1 (the catalytic subunit of RNAPI, II, and III, respectively) at DSBs was examined. The results revealed, as shown in Figure 1B, that RPC1 localized to DSBs, whereas RPA1 and RPB1 did not. The fluorescence assays in real time also indicated that RPC3, 4, 6, and 7 subunits of RNAPIII localized to DSBs (Figure 1C). Additionally, RPABC1 and 4 (the subunits shared by RNAPI, II, and III) were localized to DSBs, but RPB3 (a subunit belonging to only RNAPII) did not (Figures S1A and S1B). These results suggest that only RNAPIII localizes to DSBs. Furthermore, the RPC1 immunostaining signal was detected during the first minute after DNA breaks and quickly rose to a maximum level at around the fifth minute (Figure 1D). As shown in Figure 1C, in living cells, EGFP-tagged RPC3, 4, 6, and 7 localized to DSBs within the first minute after laser irradiation. In Figure S1C, more living cells showed the localization of RPC3, 4, 6, and 7 to DSBs in real time. The statistics shown in Figure S1C indicate the relative increase of EGFP-RPC3 or -RPC6 fluorescence at laser stripe over time and the ratio of examined cells showing RPC3, 4, 6, and 7 localized to DSBs. Taken together, these results suggest that RNAPIII is localized to DSBs, and it occurs during the very early stage of the DSB repair process. Using a similar assay, NBS1 (a subunit of MRN) and RPA32 (a subunit of RPA) were found at DSBs within the first minute after irradiation (Figures S1D and S1E). We also found that the chromatin level of the RNAPIII-specific subunit RPC7 remarkably increases in cells treated with the DSB-inducing agent Camptothecin (CPT) or etoposide (VP-16), as shown in Figure 1E, which further supports that RNAPIII localizes to DSBs. Additionally, using a single clean I-SceI-generated DSB site, chromatin immunoprecipitation (ChIP)-qPCR analysis further confirmed that RNAPIII localizes to DSBs. The construction of a 3FLAG-tagged RPC3 cell line using the CRISPR-Cas9 technique is shown in the schematic in Figure 1F. Three independent homozygous cell lines were obtained, and they showed similar growth rate compared to wild-type (WT) cells (data not shown). An IP assay showed the interaction of 3FLAG-RPC3 and RPC7, and a ChIP assay demonstrated the enrichment of 3FLAG-RPC3 in the 5S RNA and $tRNA^{Tyr}$ genomic regions in which RNAP III catalyzes transcription (Figure 1G). These results indicated that 3FLAG-RPC3 is able to integrate into the RNAPIII complex. The results in Figure 1H reveal that RNAPIII (RPC3) was enriched at the I-SceI break site. However, RNAPI (RPA1) and II (RPB1) were not enriched at the I-SceI break site, as indicated by the lack of statistically significant difference between the association of RPA1 or RPB1 with the I-SceI site before and after DNA break (Figure 1H). Additionally, the results in Figure 1H also indicate that a certain amount of RNAPII (RPB1 subunit) may exist near the I-SceI break site, which is consistent with the ubiquitous presence of RNAPII on chromatin, as required for mRNA transcription. The enrichment of RPC3 at AsisI break sites located in non-transcription regions (compacted chromatin) was also detected (Figure 1I). These results indicate that RNAPIII localizes to DSBs in both euchromatin and heterochromatin regions. Immunostaining analysis of γ-H2AX, Cyclin A2, and RPC1 in laser micro-irradiated cells revealed, as shown in Figure 1J, that RPC1 signal co-localized with γH2AX signal in both cyclin A2 (S/G2-phase-specific cyclin)-positive and -negative cells. This suggests that RNAPIII is recruited to DSBs in cells at the G1, S, and G2 phases. Taken together, these results indicate that RNAPIII, but not RNAPI and II, localizes to DSBs independent of the cell-cycle phase.

Nascent RNA synthesis and formation of RNA-DNA hybrids at DSB sites

Considering that RNAPIII localizes to DSBs, it is reasonable to anticipate that the biochemical function of RNAIII at DSBs is to catalyze RNA synthesis. Using the uracil analog 5-ethynyl uridine (5-EU) incorporation assay, newly synthesized RNAs were detected at the laser micro-irradiated stripe, which is co-localized with γH2AX (Figures 2A and S2A). We refer to this newly synthesized RNA as DSB-RNA (DNA double-strand break RNA). To determine whether the DSB-RNA is associated with a complementary DNA strand to form RNA-DNA hybrids, a fluorescence assay was performed using S9.6 antibody, a monoclonal antibody that specifically recognizes RNA-DNA hybrids (Boguslawski et al., 1986). The result in Figure 2B shows that RNA-DNA hybrids were formed at DSBs, and their signal clearly overlaps with γH2AX (Figure 2B). The formation of RNA-DNA hybrids was further examined in living cells in real-time mode, using an EGFP-HB-NLS fusion protein to recognize and detect RNA-DNA hybrids. Adding a nuclear localization signal (NLS) to EGFP-HB (a RNase H1-derived RNA-DNA hybrids binding domain fused to EGFP) remarkably increases the localization of EGFP-HB in the nucleus and considerably enhances the resolution of its fluorescence signal, compared with the only HB domain reported previously (Bhatia et al., 2014).

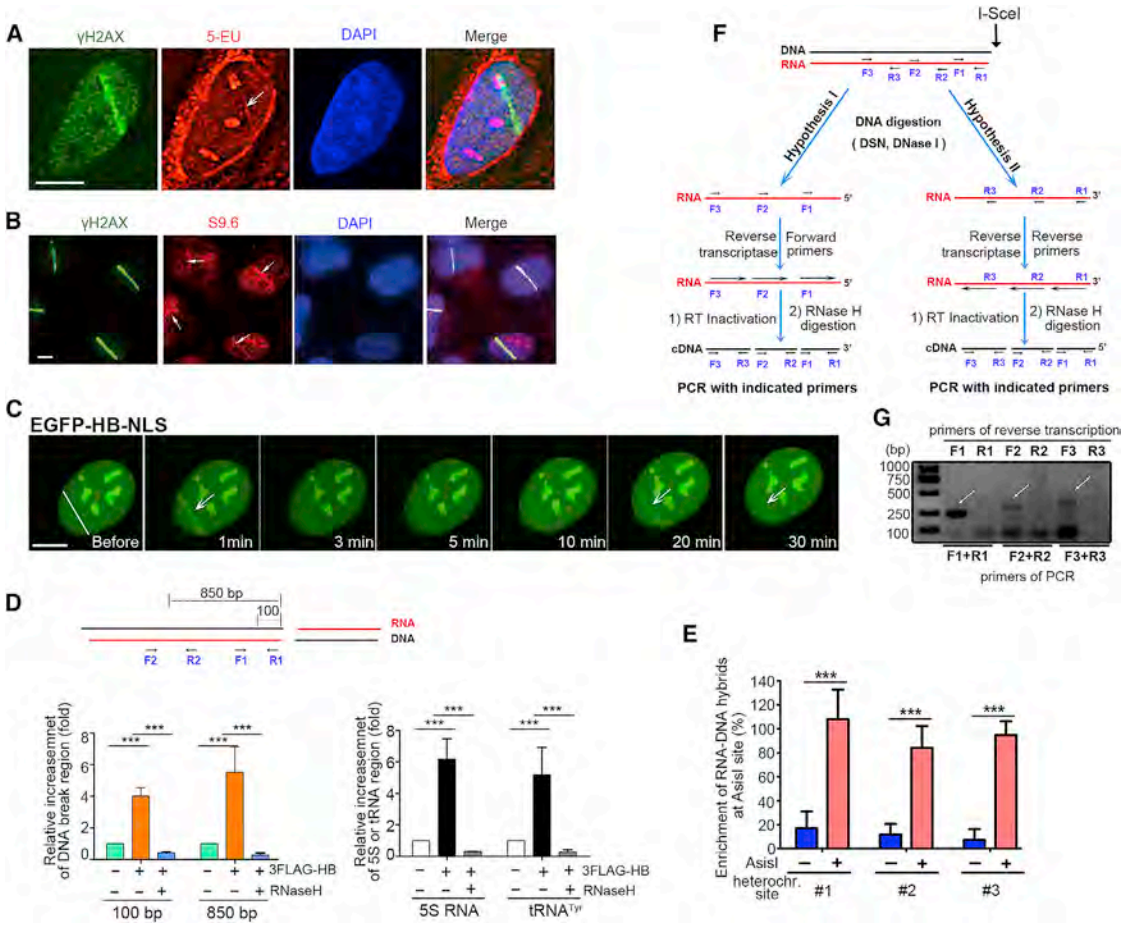

Figure 2. Detection of RNA-DNA hybrids at DSBs

(A) The detection of RNA synthesis at DSBs. The synthesis of RNA at DSBs was detected by the incorporation of 5-EU. γH2AX was detected by a specific antibody. The white arrow indicates the newly synthesized RNA at DSBs.

(B) The detection of RNA-DNA hybrids at DSBs using the S9.6 antibody. The laser-irradiated cells were stained with the S9.6 antibody and a specific antibody against γH2AX.

(C) The time point for the formation of RNA-DNA hybrids at DSBs. EGFP-HB-NLS was constitutively expressed in U2OS cells. The kinetics of EGFP-HB-NLS localization to DSBs was monitored in real time after laser microirradiation. The scale bar is 10 μm.

(D) The detection of RNA-DNA hybrids at DSBs by 3FLAG-HB affinity chromatography. Genomic DNA was prepared 15 h after transfection of the I-SceI expression plasmid. Genomic DNA, in the presence or absence of RNaseH treatment, was sonicated to an average size of ~500 bp. The RNA-DNA hybrids were then captured using a 3FLAG-HB column and subsequently quantified by qPCR to examine the abundance of RNA-DNA hybrids at the I-SceI site and 5S RNA and tRNA gene regions.

(E) Enrichment of RNA-DNA hybrids at the AsisI sites #1, 2, and 3 located in compacted chromosomal regions (for the exact sites, see Figure 1I).

(F and G) The identification of the RNA strand in the RNA-DNA hybrids at the I-SceI break site. As in Figure 2D, the RNA-DNA hybrids were captured by 3FLAG-HB affinity chromatography and subsequently subjected to DNA digestion by DSN and DNase I. The left RNA strands were reverse transcribed with the indicated primers. After heat inactivation of reverse transcriptase (70°C, 35 min), RNA was degraded by RNase H digestion (E), and the cDNA product was detected by PCR (F).

For significance analysis, we used two-paired Student's t tests. For (A)–(C), about two dozen cells were examined for each panel. See also Figure S2.

As shown in Figure 2C, a strong EGFP-HB signal appeared at the laser micro-irradiated stripe during the first minute after the DNA breaks, but the signal decreased to the lowest level at around the third or fifth minute. Afterward, the EGFP-HB signal increased again, and its extent was apparently stronger at the 10th, 20th, or 30th minute, compared to the signal at the third to fifth minute. The formation of RNA-DNA hybrids at DSBs was also examined with cells overexpressing RNase H. As shown in Figure S2B, the EGFP-HB signal appeared at laser stripes in normal S/G2 cells (expressing cyclin A2, but RNH1 not overexpressed). However, when RNH1 was overexpressed, the ratio of the S/G2 cells showing EGFP-HB signal significantly decreased, and the intensity of fluorescent signal at laser stripe also became much weaker, indicating again that RNA synthesis at DSBs takes place.

The formation of RNA-DNA hybrids at DSBs was further examined at a single DNA break site generated by cutting with I-SceI. A cell line harboring a single I-SceI endonuclease site was created by engineering an I-SceI recognition site in the second

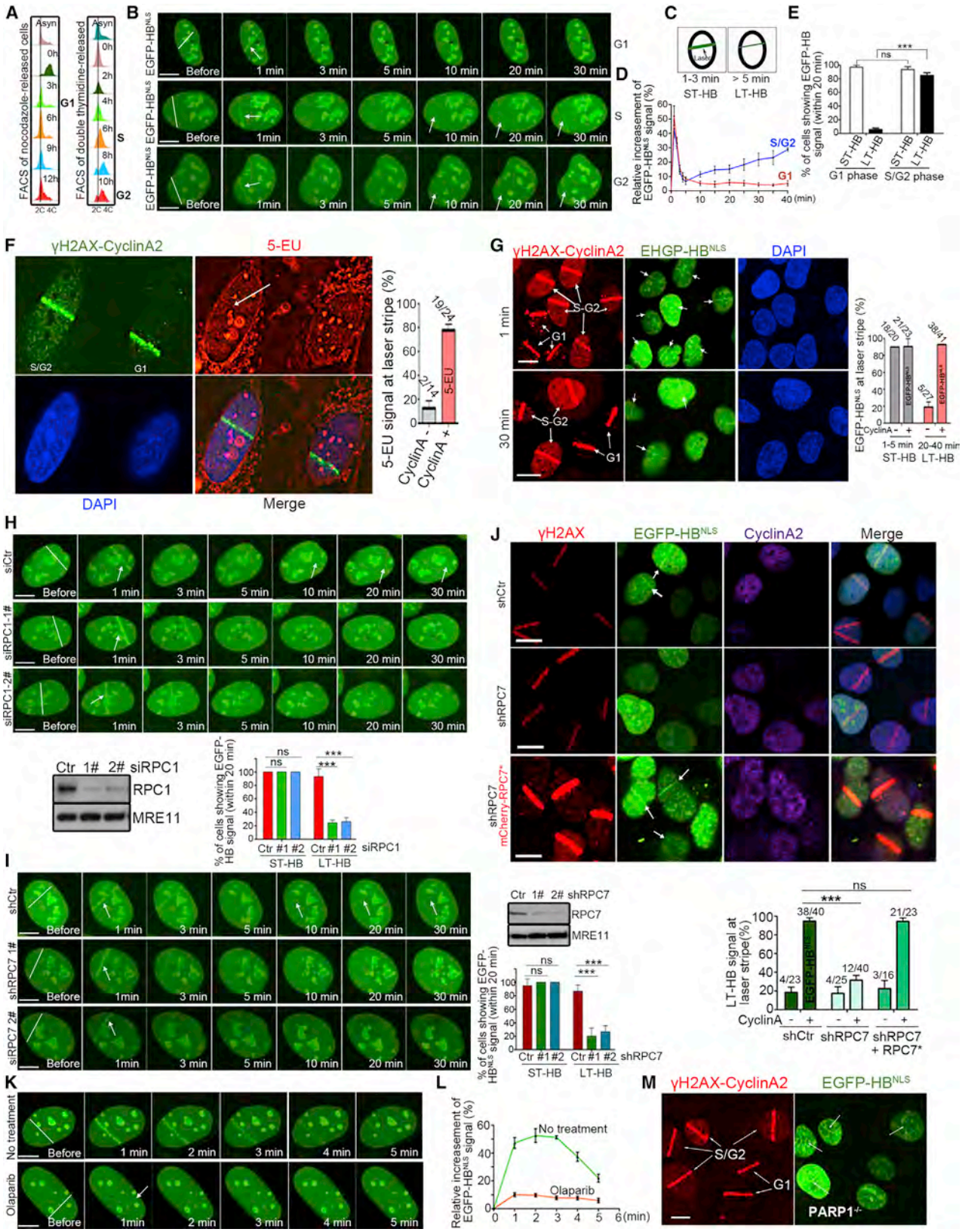

(legend on next page)

intron region of the GAPDH gene and named as GAPDH-I-SceI cell line. Fifteen hours after transfecting the GAPDH-I-SceI cells with plasmids expressing I-SceI, genomic DNA was prepared and subsequently sonicated to an average size of ~500 bp. Then, DNA-RNA hybrids were captured by the recombinant 3FLAG-HB protein affinity column before and after RNase H treatment. The captured RNA-DNA hybrids were quantified by qPCR. As shown in Figure 2D (left panel), the results reveal that the amounts of DNA captured by 3FLAG-HB-beads increased by approximately 4- to 6-fold at DNA break regions (50 or 800 bp away from the I-SceI site) compared with that captured by anti-FLAG-IgG control beads. However, this increase disappeared when the genomic DNA was treated by RNase H prior to the 3FLAG-HB affinity chromatography (Figure 2D). As a control, the highly transcribed genomic DNA regions encoding 5S RNA and $tRNA^{Tyr}$ were also enriched by 5- to 6-fold, but the enrichment also vanished when the genomic DNA was previously treated by RNase H (Figure 2D, right panel), validating the current method of using 3FLAG-HB for capturing RNA-DNA hybrids. Thus, at the clean I-SceI-generated DNA break site, RNA-DNA hybrids are also formed. Consistent with RNAPIII localized to DSBs in compacted chromatin regions (Figure 1I), the RNA-DNA hybrids were also formed at those AsisI break sites (Figure 2E).

To determine which DNA strand, the 3′- or 5′-ended strand at DSBs, is used for the formation of the RNA-DNA hybrids at DSBs, an assay, depicted in Figure 2F, was performed. The RNA-DNA hybrid(s) formed at the I-SceI break site were isolated by 3FLAG-HB affinity chromatography as shown in Figure 2D. The isolated RNA-DNA hybrids were then digested with duplex-specific nuclease (DSN) and DNase I to remove the DNA strand. The remaining RNA strand was subjected to one round of reverse transcription in a single direction with either forward primers (hypothesis I: the RNA strand was transcribed using the 3′-ended DNA strand at DSBs) or reverse primers (hypothesis II: the RNA strand was transcribed using the 5′-ended DNA strand at DSBs). After reverse transcription, the reverse transcriptase was inactivated by heat; the RNA strand was removed by RNase H digestion. Finally, PCRs were performed to analyze the reverse transcription products. As shown in Figure 2G, the forward primers (hypothesis I) generated strong DNA signals, but the reverse primers (hypothesis II) did not. This result indicates that the RNA strand in the RNA-DNA hybrids at DSBs is transcribed using the 3′-ended DNA strand. Additionally, this result is also consistent with the finding that the 5′-ended DNA strand is degraded during end resection by Exo1 and Dna2, while the 3′-ended strand remains intact. Since the R1 primer is located 35 nt away from the I-SceI site, a PCR product resulting from the R1 and F1 primers indicates that the RNA strand in the RNA-DNA hybrids is transcribed from the beginning of the very end of the 3′-ended ssDNA strand.

The formation of RNA-DNA hybrids at DSBs occurs in cells at the S and G2-M phases

To determine whether the formation of RNA-DNA hybrids is specifically related to the cell-cycle phase, the U2OS cells stably expressing EGFP-HB-NLS were first arrested at the G1/S phase by double-thymidine treatment and then released to S and G2 phase (6 and 10 h after G1/S release). For cells at the G1 phase, the U2OS cells were arrested at G2/M phase in the presence of nocodazole and then released to G1 phase (4 h after G2/M-phase release) (Figure 3A). These cells were subjected to laser micro-irradiation, and the fluorescence signals of EGFP-HB-NLS were recorded in real time in living cells. As shown in Figure 3B, the EGFP-HB-NLS signal in the cells at the G1 phase appeared within the first min, and then it quickly decreased and became hardly detectable at the fifth minute and beyond. For the cells at the S and G2 phases, the EGFP-HB-NLS signal also appeared during the first minute and then decreased to a hardly detectable level at the third and fifth minute, which is just like the cells at the G1 phase. However, as in Figure 2C, a second EGFP-HB-NLS signal appeared after the fifth minute and was detectable at the examined 10^{th}, 20^{th}, and 30^{th} min (Figure 3B). This second EGFP-HB-NLS signal could last for more than 40 min and was designated as the long-term HB signal (LT-HB) (Figure 3C), while the first EGFP-HB-NLS was designated as short-term HB signal (ST-HB) (Figure 3C). To see the two EGFP-HB-NLS signals clearly, the fluorescent images taken,

Figure 3. The requirement of RNA polymerase III for the formation of RNA-DNA hybrids at DSBs

(A) The flow-cytometry analysis of U2OS cells stably expressing EGFP-HB-NLS. The cells were arrested at G2/M or G1/S with nocodazole or double-thymidine treatment and then released to the G1, S, or G2 phase at the indicated time.

(B and C) The detection of two HB fluorescent signals, short-term HB signal (ST-HB) and long-term HU signal (LT-HB), in real time after laser irradiation in U2OS cells. The ST-HB signal appears in all cell-cycle phases in the first 1–3 min; the LT-HB signal appears only in the S and G2 phases 5 min and beyond after laser irradiation.

(D) The relative change of EGFP-HB-NLS fluorescent signal in G1, S, and G2 cells versus time after laser irradiation.

(E) The percentage of cells showing ST-HB or LT-HB signals in G1, S, or G2 phase of cells.

(F) Left, the synthesis of RNA at DSBs in S/G2 cells but not in G1 cells. RNA synthesis and γH2AX signal were detected by 5-EU incorporation and immunostaining with a specific antibody, respectively. Cyclin A2 is expressed in cells at the S and G2 phases of cells. Middle, the cells showing 5-EU signal at laser stripe. Right, the ratios of cells showing 5-EU signal.

(G) The LT-HB signal at DSBs shows only in the S/G2 cells.

(H and I) The LT-HB signal is drastically reduced in the siRPC1- or shRPC7-treated cells; the level of RPC1 or RPC7 in the siCtr-, siRPC1 (oligos #1 and 2)-, or shRPC7 (#1 and #2)-treated cells and the ratios of cells showing ST-HB or LT-B signal are also shown (bottom panels in H and right panels in I).

(J) The recovery of EGFP-HB signal after the expression of irrepressible RPC7* in the shRPC7-treated cells.

(K and L) A dramatic reduction of the ST-HB signal at DSBs in the Olaparib-treated cells (K) and the relative extent of ST-HB signal versus time after laser irradiation in the Olaparib-treated or -untreated cells (L).

(M) The PARP1 gene knockout cells were used for this assay. The EGFP-HB-NLS signal was detected at DSBs in cells at the S/G2 phase but not in G1 phase. For each florescent assay, about 20 cells were examined, or the number of examined cells is indicated in the panel. Data are represented as mean ± SD. The two-paired Student's t tests were used to analyze statistical significance. The scale bar is 10 μm. See also Figure S3.

respectively, at the first and 30th minute in Figure 3B are enlarged and presented in Figure S3A. Compared to ST-HB, LT-HB is relatively weaker (Figures 3B–3D). The percentage of cells showing ST-HB and LT-HB signals at G1, S, or G2 phase is presented in Figure 3E. The LT-HB signal was also detected in a small percentage of cells assumed to be at the G1 phase (Figure 1E), which may be due to the release of some cells from cell-cycle synchronization. The dynamics of ST-HB and LT-HB signals is shown with a movie (Videos S1 and S2).

To evaluate the biochemical properties of the two HB signals—the ST-HB and LT-HB at DSBs, we first examined the RNA synthesis at laser-irradiated stripe based on 5-EU incorporation in the cells at different phases. The results revealed that the RNA synthesis at laser-irradiated stripes occurred only in cells at the S/G2 phase that show the presence of cyclin A2 (Figure 3F). The RNA synthesis was not detected in cells at the G1 phase (Figure 3F). Using an EGFP-HB-NLS fusion protein to detect RNA-DNA hybrids at laser-irradiated stripes, the ST-HB signal was detected in both G1 and S/G2 cells at the first minute after laser irradiation, but the LT-HB was detected only in the S/G2 cells when the images were taken at the 30th minute (Figure 3G). The ratio of cells showing the ST-HB or LT-HB signal is presented in the right panels of Figures 3F or 3G, respectively. A small percentage of cells, which were assumed to be cyclin A^- cells, also showed the LT-HB signal at laser stripe (Figure 3G, right). The reason for that may be due to that these cells were actually at early to middle S phase, but the level of cyclin A was still quite low, and these cells were categorized as G1 phase of cells. A small percentage of cells with cyclin A^+ did not show the LT-HB signal or RNA synthesis at laser stripes (Figures 3F or 3G, right panels), which should be due to that some cells were severely damaged during laser irradiation.

It was found that the LT-HB signal was significantly decreased in the RNAPIII (RPC1 or RPC7 subunit) knockdown cells (Figures 3H and 3I). Enlarged images at the first or 30th minute in Figures 3H and 3I are presented in Figure S3B. The level of RPC1 or RPC7 in the siRPC1- or shRPC7-treated cells is shown in Figure 3H, bottom-left panel, and Figure 3I, top-right panel. The cell growth cycle in the siRPC1- or shRPC7-treated cells was not noticeably affected with respect of unsynchronized cell growth and double-thymidine arresting and release, compared to the untreated cells (Figures S3C and S3D). The ratios of cells showing the ST-HB or LT-HB are presented in Figure 3H, bottom-right panel, and Figure 3I, bottom-right panel. When RPC7*, which cannot be inhibited by shRPC7, was expressed in the shRPC7-treated cells, the EGFP-HB signals at laser stripes were recovered (Figure 3J). Taken together, these results indicate that the LT-HB signal results from the binding of EGFP-HB-NLS to the RNA-DNA hybrids at DSBs in which the RNA strand is newly synthesized by RNAPIII.

To determine what causes the ST-HB signal at DSBs, a few inhibitors were tested, including DRB (5, 6-dichloro-1-β-D-ribofuranosyl-1H-benzimidazole) that inhibits transcription elongation catalyzed by RNAPII and Olaparib that inhibits poly (ADP-ribose) polymerase (PARP). The inhibition analysis revealed that DRB slightly reduced the intensity of the ST-HB fluorescent signal by ~15% (data not shown), suggesting that RNAPII and its catalyzing RNA transcription should not be the main cause for the ST-HB signal, which is consistent with the finding that RNAPII is not localized to DSBs (Figures 1B and 1H; Figure S1B). The ~15% reduction of the ST-HB signal may be due to the inhibition of ongoing RNA transcription that happens to be around the laser micro-irradiated stripe. Poly (ADP-ribose) polymerization is an early event that is catalyzed by poly(ADP-ribose) polymerase (PARP) for the recruitment of DSB repair proteins to DSB sites (Beck et al., 2014; Wei and Yu, 2016). Since, structurally, the poly(ADP-ribose) chain is quite similar to a DNA or RNA chain, we tested whether the inhibition of poly (ADP-ribose) polymerization affects the ST-HB signal. It was found that Olaparib dramatically decreased the ST-HB signal to nearly a background level (Figures 3K and 3L). This result suggests that poly(ADP-ribose) chain is recognized by EGFP-HB-NLS for generating the ST-HB signals. In addition, in a PARP1 knockout cell line in which 85%–90% of poly(ADP-ribose) modification is abolished (Bai and Cantó, 2012), the EGFP-HB signal was detected only in the cells at the S and G2 phases (Figure 3M). Thus, these results indicate that the LT-HB signal reflects the RNA-DNA hybrids structure that is formed at DSBs specifically in the cells at the S and G2 phases. And RNAPIII catalyzes the synthesis of the RNA strand in the RNA-DNA hybrids.

RNA polymerase III is actively recruited to DSB sites by MRN complex

Since previous searching for additional HR proteins suggested that RNAPIII may associate with MRN during DSB repair, before investigating the mechanism by which RNAPIII is recruited to DSBs, we first confirmed the interaction between RNAPIII and the MRN complex. To this end, we performed an IP experiment against RPC3-3FLAG (3FLAG is tagged to the C-terminal of RPC3 endogenously by CRISPR-Cas9) with nuclear extracts prepared from VP16-treated cells. MRE11 was detected in the brought-down fraction (Figure 4A, left). As expected, RPC7 was also found in the brought-down fraction with IP against RPC3-3FLAG (Figure 4A, left). In the VP16-untreated cells, MRE11 was undetectable in the brought-down fraction (Figure 4A, left), suggesting that the amount of RPC3 associated with MRE11 significantly increased after DNA break. A reciprocal IP experiment confirmed the interaction between MRE11 and RPC3-3FLAG (Figure 4A, right). Furthermore, the yeast two-hybrid (Y2H) assay was used to determine the subunits in RNAPIII and the MRN complex that bring them together. All 17 subunits of RNAPIII (fused to Gal4 activating domain) and three MRN subunits—MRE11, RAD50, and NBS1 (fused to Gal4 DNA binding domain)—were screened. The results displayed in Figure 4B show that the yeast cells co-transfected with MRE11 and RNAPIII-specific subunit RPC4 or RPC6 could grow on four dropout medium (Leu^-, Trp^-, His^-, Ade^-). This result suggests that there is a basic level of interaction between RNAPIII and MRN complex through the Mre11 subunit in MRN and the RPC4, 6 subunits in RNAPIII. When DSBs occur, this interaction may recruit RNAPIII to DSBs.

To examine whether the MRN complex is responsible for recruiting RNAPIII to DSBs, the level of RPC7 on chromatin was measured in the VP16-treated and MRE11 knockdown cells. As shown in Figure 4C, the amount of RPC7 on chromatin was remarkably increased when DSBs were induced in the presence

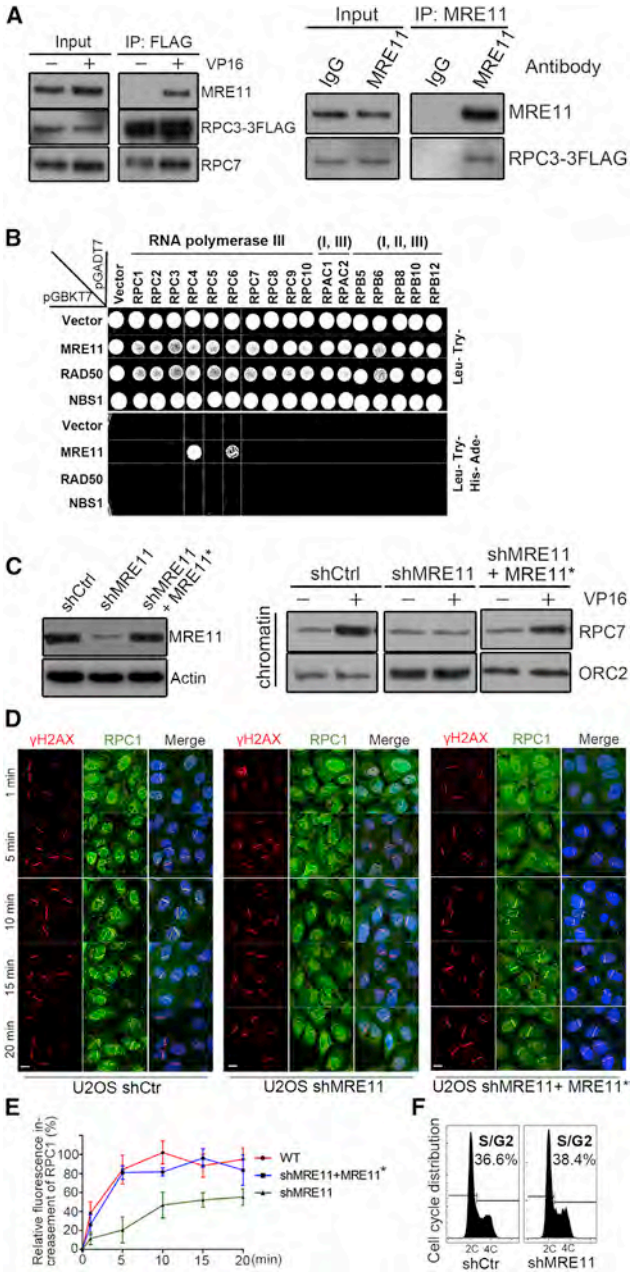

Figure 4. Requirement of the MRN complex for the recruitment of RNA polymerase III to DSBs

(A) A reciprocal immunoprecipitation (IP) showed the interaction between MRE11 and RPC3. Chromatin extracts were prepared from VP16-treated or -untreated cells. The IPs were performed with the FLAG antibody against RPC3-3FLAG, a specific antibody against MRE11, or IgG. The western blotting results are shown.

(B) A yeast two-hybrid (Y2H) assay reveals the interaction of MRN and RNA polymerase III via Mre11 and RPC4 and RPC6 subunits of RNAPIII. Each of the 17 subunits of RNAPIII was fused to the Gal4 activation domain, and the MRE11, RAD50, and NBS1 subunits of MRN complex were individually fused to the Gal4 DNA binding domain. The Y2H assay was conducted routinely.

(C) The accumulation of RPC7 in chromatin in the VP16-treated cells was decreased in the shMRE11-treated cells but recovered when a shMRE11-undegradable form of MRE11* was expressed. Left: the amount of MRE11 in the shCtrl-, shMRE11-, or shMRE11-treated + MRE11*-expressed cells. Right: the amount of RPC7 accumulated in chromatin in VP16-treated or -untreated cells. The western blotting results are shown.

(D) The fluorescence intensity of RPC1 decreased in shMRE11-treated cells. Fluorescence intensity of γH2AX and RPC1 was measured at the indicated time after laser microirradiation in shCtrl-, shMRE11-, and shMRE11 + MRE11*-treated cells.

(E) Statistical analysis of increased RPC1 florescent intensity at DSBs compared to background in nuclei. RPC1 was detected with a specific antibody.

(F) The distribution of cell-cycle phases was not altered in the shMRE11-treated cells, compared to shCtr-treated cells, by flow-cytometry analysis.

At least two dozen cells were examined in fluorescent analysis. Data are represented as mean ± SD. The scale bar is 10 μm.

of VP16. However, this increase was no longer detected when the cellular amount of MRE11 was depleted by approximately 80% in the shMRE11-treated cells. The level of RPC7 in chromatin was restored when a shMRE11-resistant MRE11* was overexpressed in the MRE11-depleted cells (Figure 4C). Additionally, the fluorescence intensity of RPC1 at DSBs decreased significantly in the shMRE11-treated cells, but the RPC1 fluorescence signal recovered when shMRE11-resistant MRE11 was expressed in the cells (Figures 4D and 4E), which supports an essential role of MRN in recruiting RNAPIII to DSBs. As shown in Figure 4F, the distribution of cell-cycle phases was not altered in the MRE11 knockdown cells. Taken together, these results indicate that RNAPIII is actively recruited to DSBs by the MRN complex.

CtIP and MRN nuclease activity is required for the generation of RNA-DNA hybrids at DSBs

To investigate whether end resection plays a role for the RNA-DNA hybrid formation at DSBs, we developed a CtIP knockout (KO) U2OS cell line (Figures 5A–5C), using CRISPR-Cas9 technique targeting the sixth exon (176 bp). There are three CtIP alleles in U2OS cells (Przetocka et al., 2018). Sequencing analysis indicated that this CtIP knockout cell line has a single base " T " insertion in two CtIP gene alleles and a 151-bases insertion including 24 repeats of the telomere sequence TTAGGG in the third allele, based on the levels of PCR products (the ratio of a′: b′ is approximately 2:1), as shown in Figures 5A and 5B. Both mutations occur at the guide RNA targeted site, and they cause an open reading frame (ORF) shift (Figure 5B). Unexpectedly, western blotting analysis detected a slight amount (~1/40 of WT level) of CtIP in the CtIP gene knockout cells (Figure 5C). This small amount of CtIP, which may result from a rare alternative splicing of mRNAs, supports cell growth, as CtIP is known to be essential for cells. An experiment in this CtIP-KO cell line showed that the recruitment of RNAPIII to DSBs was not affected (Figures S4A and S4B). However, the formation of the LT-HB signal was dramatically reduced in the CtIP KO cells at the G2 phase but recovered when a wild-type CtIP was expressed (Figures 5D and 5E). As expected, the ST-HB signal was not affected (Figures 5D and 5E). The fluorescent images at the first and 30th minute in Figure 5D are enlarged and presented in Figure S4E, in order to see the LT-HB and ST-HB signals more clearly. Flow-cytometry analysis indicated that, compared to wild-type cells, the cell-cycle distribution did not noticeably

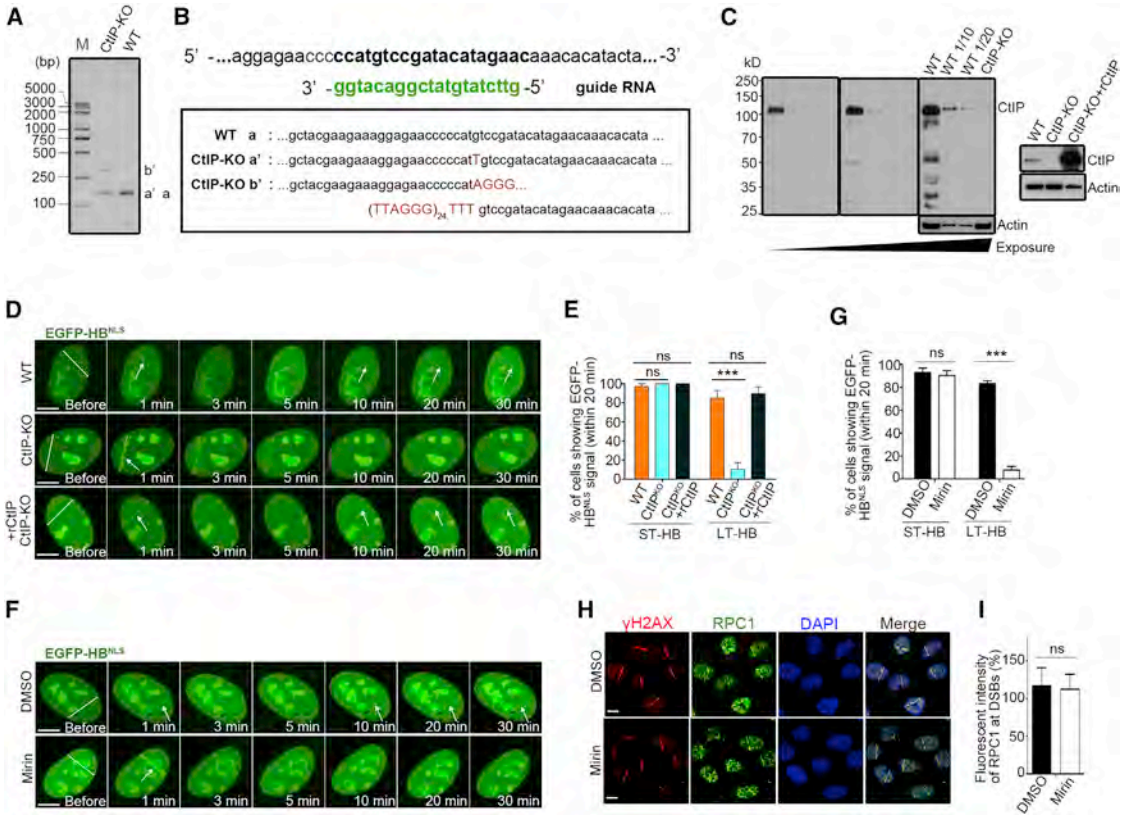

Figure 5. Requirement of CtIP and the exonuclease activity of MRE11 for the formation of RNA-DNA hybrids at DSBs

(A and B) The mutations of CtIP gene in the CtIP knockout (KO) cell line. The U2OS cell line harbors three copies of CtIP gene. (A) Two fragments, a′ and b′ bands in agarose gel, were obtained in a PCR by amplifying a DNA region of CtIP gene containing the CRISPA-Cas9-targeted site in CtIP-KO cell line.

(B) DNA sequencing showed that the a′ fragment has a T base insertion and the b′ fragment has 151-base insertion at the CRISPR-Cas9 targeted site. Both mutations cause an open reading frameshift.

(C) The amounts of CtIP in wild-type (WT), CtIP-KO, and CtIP-KO + CtIP-overexpressing cells.

(D and E) Requirement of CtIP for the formation of RNA-DNA hybrids. (D) The images of EGFP-HB-NLS signal versus time after laser irradiation in WT, CtIP-KO, and CtIP-KO + CtIP-overexpressing cells. (E) Statistical measurement of EGFP-HB-NLS signal in the cells.

(F and G) Requirement of MRE11 exonuclease activity for the formation of RNA-DNA hybrids at DSBs. The EGFP-HB-NLS fluorescence images at DSBs (F) and statistical measurement of the EGFP-HB-NLS signal in Mirin-treated or -untreated (DMSO) cells (G).

(H) The recruitment of RPC1 was not affected in Mirin-treated cells. Left, fluorescence images; right, the statistical measurement of RPC1 fluorescence intensity at DSBs in DMSO or Mirin-treated cells.

At least two dozen cells were examined in fluorescent analysis. Data are represented as mean ± SD. Statistical analyses were performed with an unpaired two-tailed Student's test. *$p \leq 0.05$; **$p \leq 0.01$; ***$p \leq 0.001$. The scale bar is 10 μm. See also Figure S4.

change in the CtIP-KO cells (Figure S4C). The synchronization by double-thymidine and release was not altered either for the CtIP KO cells (Figure S4D), compared to WT cells (Figure 3A).

Moreover, the inhibition of MRE11 exonuclease activity by Mirin also abolished the LT-HB signal (Figures 5F and 5G; see enlarged images in Figure S4F), but the ST-HB signal was not affected (Figures 5F and 5G). But the fluorescence analysis of RPC1 indicates that the localization of RPC1 to DSBs was not affected in the Mirin-treated cells (Figures 5H and 5I), suggesting that RNAPIII is normally recruited to DSBs when the MRE11 nuclease activity is inhibited. Both CtIP and Mre11 nuclease activity is required for the initiation of end resection, which removes approximately a few dozen nucleotides from the 5′-ended strand to generate a ssDNA region in the 3′-ended strand (Cannavo and Cejka, 2014; Symington and Gautier, 2011). Together, these results suggest that a limited end resection, which is catalyzed by MRN-CtIP, is required for RNAPIII-mediated RNA synthesis and the subsequent formation of RNA-DNA hybrids at DSBs. A possible reason for this is that a short ssDNA region on the 3′-strand, which is generated by MRN-CtIP-mediated end-resection initiation, is required for initiation of RNA synthesis by RNAPIII at DSBs.

Inhibition of homologous recombination and end resection in the siRPC1-treated cells

To determine whether the formation of RNA-DNA hybrids is required for HR-mediated DSB repair, we measured the rate of DSB-induced HR in cells with decreased amount of RPC1 after treatment with siRPC1, or in cells treated with 40 μM of RNAPIII inhibitor ML-60218. The experimental system used to measure the rate of DSB-induced HR is outlined in Figure 6A. When HR

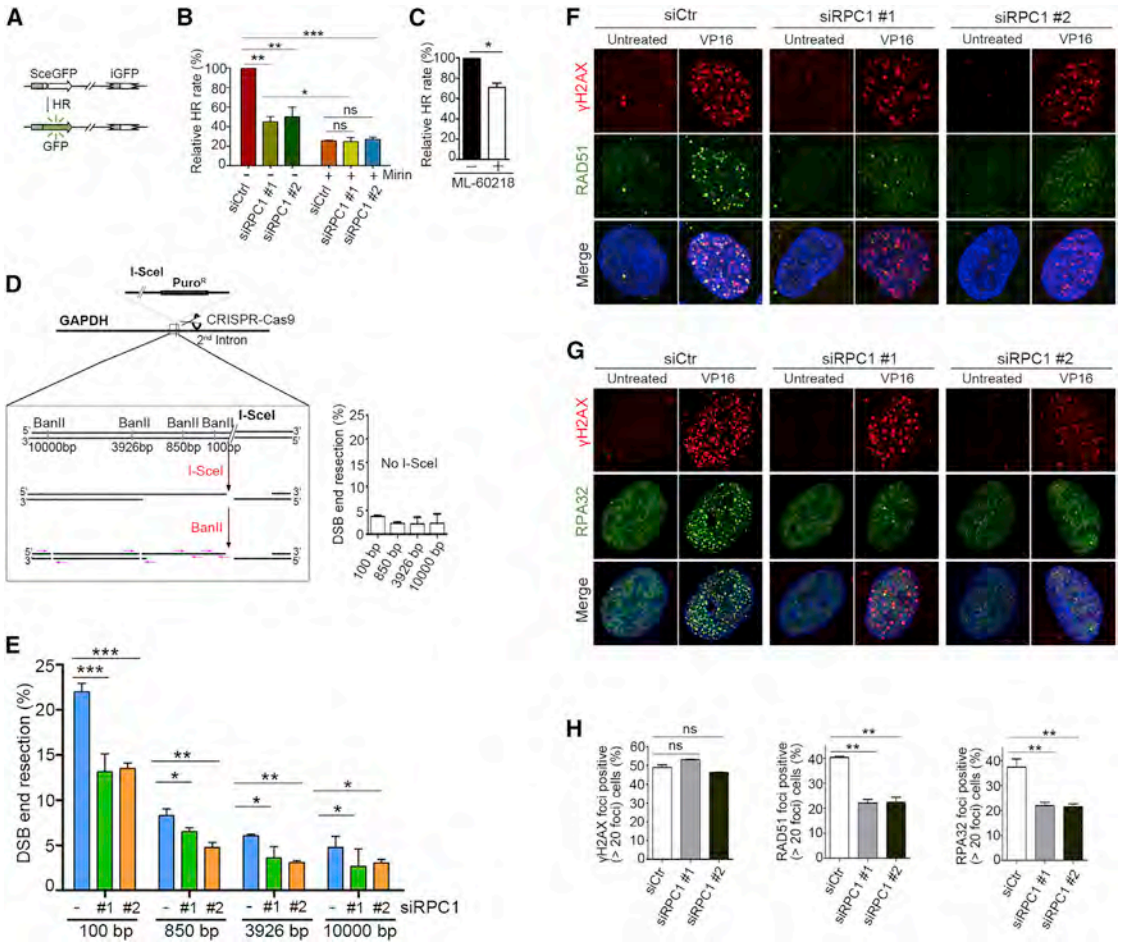

Figure 6. A reduced level of RNA polymerase III inhibits homologous recombination, end resection, and the formation of RAD51 and RPA foci

(A) Experimental system to measure the HR rate. HR will create an intact gene encoding for GFP.

(B) The rate of HR was decreased in siRPC1- or Mirin-treated cells. siRPC1 treatment did not further decrease the HR rate in the Mirin-treated cells.

(C) A reduced HR rate in the ML-60218-treated cells.

(D) Experimental system to measure end resection. Left: an I-SceI site was engineered at the second intron of the GAPDH gene. The distances of BanII sites located at the left side of I-SceI site are indicated. Right: without I-SceI cut, a similar basal level of end resection at the genomic sites that are 100 to 10,000 bp away from the I-SceI site.

(E) The efficiency of end resection in the siCtrl- or siRPC1-treated cells.

(F and G) The number of RAD51 or RPA32 foci was significantly reduced in the siRPC1-treated cells.

(H) The percentage of cells showing γH2AX foci or more than 20 foci of RAD51 or RPA32 in a single cell.

At least two dozen cells were examined in fluorescent analysis. For (H), at least 50 cells were examined. Data are represented as mean ± SD. Statistical analyses were performed with an unpaired two-tailed Student's test. *p ≤ 0.05; **p ≤ 0.01; ***p ≤ 0.001. The scale bar is 10 μm.

occurs, an intact gene encoding the GFP protein is generated (Pierce et al., 2001). As shown in Figures 6B and 6C, a decreased level of RPC1 by siRPC1 or inhibition of RNAPIII by ML-60218 reduced the rate of HR by nearly 50% and 30%, respectively. The rate of HR was further decreased when the cells were treated with both siRPC1 and Mirin, compared with cells treated only with siRPC1 (Figure 6B). However, in the Mirin-treated cells, additional siRPC1 treatment did not further decrease the HR rate (Figure 6B). These results indicate that RNAPIII and the nuclease activity of the MRN complex are required for HR. Taking the results presented here and in Figures 4 and 5, we conclude that RNAPIII functions after end-resection initiation by MRN-CtIP.

To gain further insight into the mechanism requiring the formation of RNA-DNA hybrids for HR, we first examined whether end resection is affected when either the RNA synthesis or the formation of RNA-DNA hybrids is disrupted, considering that both of these two events occur at very early stage of the HR process (Figures 1C, 1D, 2C, and 3B) (Symington and Gautier, 2011; Zhang et al., 2016). To this end, we took advantage of the GAPDH-I-SceI U2OS cell line in which an I-SceI site was inserted at the second intron of the GAPDH gene by CRISPR-Cas9 technique, as shown in Figure 6D. The four restriction enzyme BanII sites at the left side with different distances to the I-SceI site are shown. The efficiency of end resection was measured in the siRPC1- and siCtrl-treated

cells, with a method depicted in Figure 6D. When the end resection of the 5′-strand passes through BanII sites, it will generate ssDNA regions (3′ ssDNA overhang) at these BanII sites that are resistant to BanII digestion. Then, a qPCR can determine the percentage of dsDNA region at each BanII site that has been converted into ssDNA by end resection (Zhang et al., 2016). In three independent assays, the cutting efficiency at the I-SceI site was 35%–52% (data not shown). The results shown in Figure 6E indicate that the end resection was significantly reduced in the siRPC1-treated cells, compared to siCtrl-treated cells at all four examined BanII sites, which are 100, 850, 3,926, and 10,000 bp away from the I-SceI site, respectively. These results suggest that RNAPIII-mediated RNA synthesis at DSB sites significantly promotes end resection at both early and late stages, considering the end resection within ~100 or 200 bp of DNA regions around the I-SceI break site as early stage.

We also measured the formation of RAD51 and RPA32 foci in siCtr- and siRPC1-treated cells. As shown in Figures 6F and 6G, the number of RAD51 or RPA32 foci in the siRPC1-treated cells was dramatically reduced, while γH2AX foci remained almost unchanged. In addition, the percentage of cells showing more than twenty RAD51 or RPA32 foci per cell was reduced by nearly 50% in siRPC1-treated cells (Figure 6H, middle and right panels). However, a similar percentage (approximately 50%) of cells showed γH2AX foci in the siCtr- and siRPC1-treated cells (Figure 6H, left panel). DNA breaks in those assays were induced by VP16 treatment. These results further suggest that the RNAPIII-mediated DSB-RNA synthesis promotes end resection.

Genetic loss at DSBs in the siRPC1 or shRPC7-treated cells

Since the DNA strand in the RNA-DNA hybrids is the 3′ ssDNA overhang, the formation of RNA-DNA hybrids may have a direct effect on the stability of the 3′ ssDNA overhangs during end resection. To verify this, we directly examined whether genetic loss occurs at DSBs when the formation of RNA-DNA hybrids is inhibited. A hygromycin^r (*hph*) gene is located approximately 2,000 bp downstream to the I-SceI cleavage site (Figure 7A). After a DSB is generated by I-SceI cleavage, an extensive end resection, which may still be performed by EXO1 even without RNAPIII-promoted end resection but in a less extent, will remove the 5′ strand of the *hph*^{r} gene. If the generated 3′-ssDNA overhang is not protected, the cells with partial or total loss of the *hph*^{r} gene will become sensitive to hygromycin. The results shown in Figures 7B and 7C reveal that approximately 8%–9% of the cells lost the *hph*^{r} gene in the siRPC1-treated cells, while only ~3% cells lost the *hph*^{r} gene in the siCtrl-treated cells. In the presence of ML-60218, the loss rate of the *hph*^{r} gene was about 12%, while in the control cells the loss rate was about 2% (Figure 7C). The rate of *hph*^{r} gene loss was also measured in the MRN, CtIP, or RPC7 knockdown cells. Like in RPC1 knockdown cells, the RPC7 knockdown cells exhibited about a 13% *hph*^{r} loss rate, but MRN or CtIP depletion did not increase the *hph*^{r} loss rate compared to control cells (Figures 7D and 7E).

To more precisely reveal the molecular nature of genetic alterations around DSB sites in WT and siRPC1-treated cells, a DNA region of about 250 bp at each side of the I-SceI site was sequenced. Genomic DNA was prepared from cells transfected by the I-SceI expression plasmid for 24 or 72 h (Figure 7F). For the samples transfected for 24 h, the overall mutation rate was relatively low (around 1%) in siRPC1-treated or -untreated cells (Figure 7G). These mutations were further sub-grouped as point mutations, 1–3 bp indel, 4–30 bp deletion, >30 bp deletion, and >3 bp insertion. Except that the mutation of >30 bp (several dozen to several hundreds) deletion was increased by about 2-fold in the siRPC1-treated cells, the other types of mutation rates were basically the same between WT and siRPC1-treated cells (Figure 7G). For the cell samples collected 72 h after the transfection of the I-SceI plasmid, the overall mutation rate was apparently increased in both siCtr- or siRPC1-treated cells. However, the rate of mutations increased about 2-fold faster in the siRPC1-treated cells compared with siCtr-treated cells. Correspondingly, the mutation rate of >30 bp deletion was about 4- to 5-fold higher in the siRPC1-treated cells than in the siCtr-treated cells (Figure 7H). However, for the other types of mutations, there was no much difference between the siRPC1-treated cells and the siCtr-treated cells (Figure 7H). The 1- to 3-bp indel should result from the repair of DSBs by non-homologous end joining (NHEJ). A similar rate of 1- to 3-bp indel in the Ctrl- or siRPC1-treated cells suggests that the NHEJ pathway was not much affected in the siRPC1-treated cells, which is consistent with RNAPIII functioning in HR and HR-mediated DSB repair. Here, the rate of NHEJ did not increase, while the rate of HR decreased in the siRPC1-treated cells. A possible explanation is that initiation of end resection is not affected by the reduction of RNAPIII in the siRPC1-treated cells, because the localization or recruitment of CtIP and MRN to DSBs was not affected by a reduced level of RNAPIII (Figures S5A and S5B). Once end resection initiates, it will go on to either HR-mediated repair, microhomology-mediated end joining (MMEJ), or abortion of HR-mediated repair; thus, the NHEJ pathway should not be affected. Consistent with the logic, DNA sequencing in both siCtr- or siRPC1-treated cells indicates that almost all break repairs in the category of >30 bp deletion resulted from MMEJ (data not shown), because, once end resection initiates, dsDNA breaks either get unrepaired (HR abortion and cell death) or go to the MMEJ pathway for getting repaired efficiently. Taken together, these results demonstrate that RNAPIII and the formation of RNA-DNA hybrids at DSB site are required for end resection and the protection of the 3′-ssDNA overhangs.

DISCUSSION

DNA homologous recombination (HR) and HR-mediated repair of double-strand DNA breaks play a critical role in preserving genome integrity. This biological process consists of end resection, strand invasion and subsequent DNA synthesis, and resolution of Holliday junctions. The molecular mechanisms of strand invasion and resolution of Holliday junctions are relatively well established, largely due to their mechanistic similarity to the same events occurring in prokaryotes. However, the end resection in eukaryotes appears to be much more complicated, due to the chromatin structure and a strict regulation restricting end resection to the S and G2 phase of the cell-division cycle. Not much progress was made in the mechanistic study of end resection until 2008 when Dna2 and Exo1 were found to play a direct

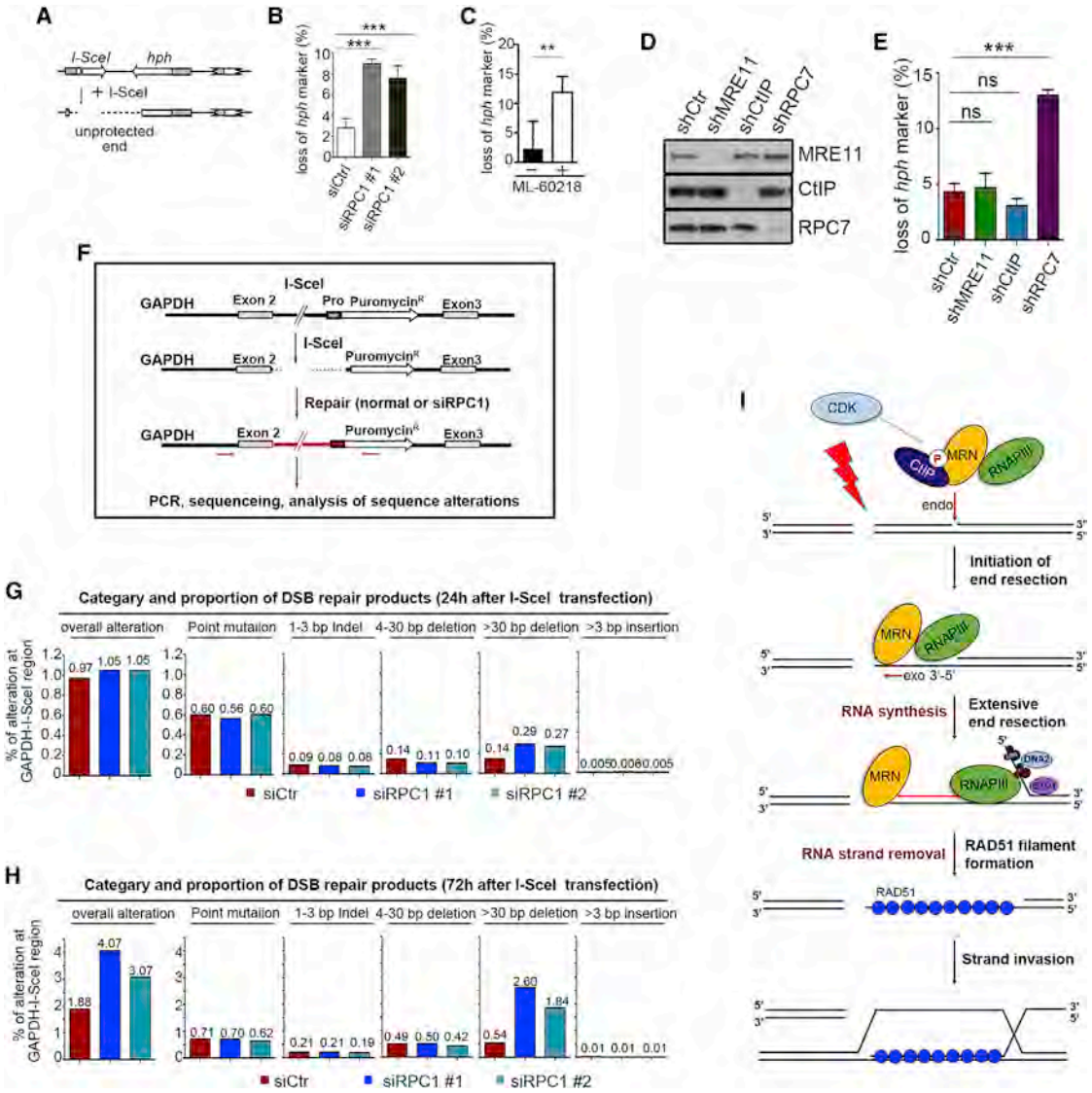

Figure 7. A reduced level of RNA polymerase III, or inhibition of RNA polymerase III activity, results in genetic deletion

(A) Experimental system for examining genetic deletion. A hygromycin^r (*hph*) gene is located about 2,000 bp away from the *I-SceI* site (DNA break site). End resection will generate a ssDNA region in the *hph* gene that requires protection from nuclease digestion.

(B and C) The percentage of cells losing a functional *hph* gene in the control cells and the siRPC1- or ML-60218-treated cells.

(D) The reduction of MRE11, CtIP, or RPC7 in the shCtr-, shMRE11-, ShCtIP-, or shRPC7-treated cell lines.

(E) The percentage of cells losing a functional *hph* gene in the shCtr-, shMRE11-, ShCtIP-, or shRPC7-treated cells.

(F) An outline of the analysis of the DNA sequence surrounding the I-SceI break site.

(G and H) The rate of various genetic mutations around I-SceI site after the treatment with siCtr, siRPC1 #1, siRPC1#2 for 24 or 72 h.

(I) A model of the formation and function of RNA-DNA hybrids. In eukaryotes, the HR-mediated repair of DSBs initiates with the binding of the MRN complex to DNA break ends. Then, RNA polymerase III is recruited to DNA break ends by the MRN complex. MRN-CtIP initiates end resection to create a short ssDNA region of about a few dozen nucleotides in the 3′-ended strand. RNA polymerase III uses the short ssDNA region as a template to start RNA synthesis. RNA synthesis will displace the 5′ strand. The displaced 5′ strand (flap structure) is degraded by flap endonuclease DNA2. The 5′ strand can also be degraded by EXO1 when it is still annealed with the 3′ strand. The synthesis of the RNA strand results in the formation of RNA-DNA hybrids that protects the 3′-ssDNA overhang against degradation by DNA2 during end resection. After end resection, the RNA strand is degraded for the subsequent formation of RAD51 filament.

Statistical analyses were performed with an unpaired two-tailed Student's test. *p ≤ 0.05; **p ≤ 0.01; ***p ≤ 0.001. See also Figure S5.

role in resecting the 5′-ended strand (Mimitou and Symington, 2008; Zhu et al., 2008). However, some critical questions related to end resection remain open. For example, a very critical question related to end resection is how the 3′-ended strands are protected during the degradation of the 5′-ended strands. The present study reveals that eukaryotic cells protect the 3′-ended strands by forming an RNA-DNA hybrid during end resection. This study also demonstrated that RNAPIII is responsible for

catalyzing the synthesis of the RNA strand in the RNA-DNA hybrid.

The detection of RNAPIII and RNA-DNA hybrids in the first minute after DSBs indicates that these events are among the first to occur in the process of DSB repair. This is consistent with the requirement that the 3′-ssDNA overhangs must be protected at the very beginning of end resection. Based on our results, we propose that, once the MRN complex binds to DSBs, the MRN complex recruits RNAPIII to DSBs. The requirement of CtIP and the nuclease activity of the MRN complex suggest that the initial resection of the 5′ strand by MRN and CtIP exposes a ssDNA region of a few dozen to ~200–300 nucleotides on the 3′ strand (Cannavo and Cejka, 2014; Mimitou et al., 2017; Zhu et al., 2008), and RNAPIII uses this ssDNA region as a template to start RNA synthesis. Previous studies have indicated that ssDNA molecules may efficiently serve as RNAPIII templates for RNA synthesis (Roeder et al., 1976; Schroder et al., 2003; Seidl et al., 2013). Continuous RNA synthesis, together with helicase action, will displace a piece of 5′ DNA strand and generate a flap DNA structure. This flap structure is an ideal substrate for DNA2 flap endonuclease. This is likely the reason that end resection was inhibited when RNAPIII was depleted by siRPC1 (Figure 6E), and RNA synthesis and the formation of RNA-DNA hybrids are correspondingly repressed (Figure 3G). Through multiple cycles of RNA synthesis and helicase action, 5′-strand displacement and generation of flap structures, and removal of flap structures by DNA2 cleavage, together with exonucleolytic digestion by EXO1, the 5′ strand is resected. Simultaneously, the RNA-DNA hybrids are formed to protect the 3′-strand overhang during end resection (Figure 7I). The promotion of end resection by RNAPIII (Figure 6E) suggests that RNA synthesis by RNAPIII plays an important role in generating flap structures for DNA2 cleavage, apart from the action of WRN and BLM helicases in generating flap structures (Sturzenegger et al., 2014). This is consistent with one of the fundamental properties of RNA polymerases-mediated transcription events—the 5′ strand is displaced as RNA polymerases move along the 3′ strand and synthesize RNA. This may explain, at least partially, why Rqh1 helicase in fission yeast is not strictly required for end resection (Langerak et al., 2011; Zhang et al., 2016).

The Dna2-mediated resection of the 5′-ended strand, as discussed above, is probably promoted by the RNAPIII-mediated RNA synthesis. However, RNAPIII should not be required for the Exo1-catalyzed end resection. Thus, under the inhibition of RNA synthesis either by reducing the level of RNAPIII (siRPC1, shRPC7) or inhibiting its activity in the presence of ML-60218, a certain level of end resection by Exo1 should still occur, resulting in a ssDNA region on the 3′-ended strand. If this ssDNA region does not have protection through the formation of RNA-DNA hybrid, it will be cut by nucleases at breaks, potentially resulting in genetic loss (Figures 7A–7H). By analyzing the types of genetic mutations around DNA break sites, it was found that only the rate of genetic deletion >30 bp increased in the siRPC1-treated cells, but point mutations, 1- to 3-bp indel, >3-bp insertion, and 4- to 30-bp deletion occurred at similar rates in the control cells and the cells with a reduced level of RNAPIII (Figures 7G and 7H). These findings suggest that NHEJ should not be affected by the depletion of RNAPIII. Since CtIP and MRE11 nuclease activity is required for the formation of RNA-DNA hybrids at DSBs (Figure 5), RNA synthesis catalyzed by RNAPIII should take place after CtIP-MRN complex initiates end resection. Therefore, the depletion of RNAPIII affects the formation of RNA-DNA hybrids, the rate of HR, and genetic integrity around DNA breaks. However, RNAPIII should not have an effect on the pathway selection of HR and NHEJ.

After end resection, the RNA strand in the RNA-DNA hybrids will be degraded for subsequent assembly of RAD51 on the 3′-ssDNA overhang. A few previous studies observed the generation of small RNAs at DSBs (Francia et al., 2012; Michalik et al., 2012; Wei et al., 2012). These small RNAs should be the degradation products of RNA strand in the RNA-DNA hybrids. Besides, the time point for the degradation of the RNA strand must be strictly regulated. A premature removal of the RNA strand, or removal before the completion of end resection, will expose the 3′-ssDNA overhang, which increases the risk of cleavage by nucleases, such as DNA2. If the RNA strand is not timely removed after end resection, the formation of RAD51 filament and subsequent repair processes will be affected. In either case, it will affect the efficiency of HR-mediated DSB repair and potentially result in genetic deletion. This may explain the findings that either the deletion of RNase H1 and RNase H2 or the overexpression of RNase H1 affects the efficiency of HR-mediated DSB repair (Ohle et al., 2016).

This study demonstrated that (1) RNA polymerase III is an essential factor in HR or HR-mediated repair of DSBs; (2) the RNA-DNA hybrid at DSB is an essential repair intermediate in the process of HR-mediated DSB repair; (3) RNAPIII is actively recruited to DSBs by the MRN complex; (4) RNAPIII is responsible for catalyzing RNA strand synthesis in the RNA-DNA hybrids; (5) both CtIP and MRN nuclease activity is required for the formation of RNA-DNA hybrids at DSBs, suggesting that a short ssDNA region on the 3′-ended strand, which is generated by the CtIP-MRN complex-mediated degradation of the 5′-ended strand, is required for initiating RNA synthesis; (6) RNAPIII promotes end resection, suggesting that RNA synthesis displaces the 5′-ended strand to generate flap structures for DNA2 digestion; and (7) the biological function of the RNA-DNA hybrids at DSBs is to protect the 3′-ssDNA overhangs during end resection. This study demonstrates that RNA polymerase III is an essential factor for the HR-mediated repair of DSBs and that the RNA-DNA hybrids at DSBs are an essential repair intermediate.

STAR★METHODS

Detailed methods are provided in the online version of this paper and include the following:

- KEY RESOURCES TABLE
- RESOURCE AVAILABILITY
  - Lead contact
  - Materials availability
  - Data and code availability
- EXPERIMENTAL MODEL AND SUBJECT DETAILS
- METHOD DETAILS
  - Cell transfection

- CRISPR-Cas9 gene editing
- Laser micro-point irradiation and immunofluorescence microscopy
- Capturing RNA-DNA hybrids at DSBs
- Immunostaining
- Immunoprecipitation assay
- Chromatin fraction extraction
- Assay of homologous recombination
- Hygromycin B sensitivity assay
- Chromatin immunoprecipitation assay
- Assay of end resection
- Sequencing analysis of DSB repair products in the siCtr- and siRPC1-treated cells

- QUANTIFICATION AND STATISTICAL ANALYSIS

SUPPLEMENTAL INFORMATION

Supplemental information can be found online at https://doi.org/10.1016/j.cell.2021.01.048.

ACKNOWLEDGMENTS

We thank all members of the Kong Laboratory for discussion and support, X. Xu (Capital Normal University) for help in laser micropoint microscopic analysis, Jun Huang (Zhejiang University) for providing DR-GFP cells that were originally from Dr. M. Jasin's lab, and X. Zhou for mass spectroscopy. This work was supported by grants from the Ministry of Science and Technology of China (2016YFA0500301 and 2013CB911000), the National Natural Science Foundation of China (no. 31230021), the Peking-Tsinghua Center for Life Sciences, and the National Key Laboratory of Protein and Plant Gene Research. We thank National Center for Protein Sciences (Beijing) at Peking University for assistance with FACS and laser micropoint irradiation assays.

AUTHOR CONTRIBUTIONS

Conceptualization, D.K.; methodology and investigation, S.L. performed most assays, including a significant portion of experimental designs; Y.H., J.W., and L.L. also made significant contributions to this study; J.Y., B.Z., and Z.W. constructed several strains; writing, review, and editing, D.K. and S.L.; funding acquisition, D.K.

DECLARATION OF INTERESTS

The authors declare no competing interests.

Received: September 6, 2019
Revised: September 24, 2020
Accepted: January 26, 2021
Published: February 23, 2021

REFERENCES

Aguilera, A., and Gómez-González, B. (2017). DNA-RNA hybrids: the risks of DNA breakage during transcription. Nat. Struct. Mol. Biol. *24*, 439–443.

Bai, P., and Cantó, C. (2012). The role of PARP-1 and PARP-2 enzymes in metabolic regulation and disease. Cell Metab. *16*, 290–295.

Beck, C., Robert, I., Reina-San-Martin, B., Schreiber, V., and Dantzer, F. (2014). Poly(ADP-ribose) polymerases in double-strand break repair: focus on PARP1, PARP2 and PARP3. Exp. Cell Res. *329*, 18–25.

Bhatia, V., Barroso, S.I., García-Rubio, M.L., Tumini, E., Herrera-Moyano, E., and Aguilera, A. (2014). BRCA2 prevents R-loop accumulation and associates with TREX-2 mRNA export factor PCID2. Nature *511*, 362–365.

Boguslawski, S.J., Smith, D.E., Michalak, M.A., Mickelson, K.E., Yehle, C.O., Patterson, W.L., and Carrico, R.J. (1986). Characterization of monoclonal antibody to DNA.RNA and its application to immunodetection of hybrids. J. Immunol. Methods *89*, 123–130.

Cannavo, E., and Cejka, P. (2014). Sae2 promotes dsDNA endonuclease activity within Mre11-Rad50-Xrs2 to resect DNA breaks. Nature *514*, 122–125.

Cejka, P., Cannavo, E., Polaczek, P., Masuda-Sasa, T., Pokharel, S., Campbell, J.L., and Kowalczykowski, S.C. (2010). DNA end resection by Dna2-Sgs1-RPA and its stimulation by Top3-Rmi1 and Mre11-Rad50-Xrs2. Nature *467*, 112–116.

Cramer, P., Armache, K.J., Baumli, S., Benkert, S., Brueckner, F., Buchen, C., Damsma, G.E., Dengl, S., Geiger, S.R., Jasiak, A.J., et al. (2008). Structure of eukaryotic RNA polymerases. Annu. Rev. Biophys. *37*, 337–352.

Daley, J.M., Niu, H., Miller, A.S., and Sung, P. (2015). Biochemical mechanism of DSB end resection and its regulation. DNA Repair (Amst.) *32*, 66–74.

Deshpande, R.A., Lee, J.H., Arora, S., and Paull, T.T. (2016). Nbs1 Converts the Human Mre11/Rad50 Nuclease Complex into an Endo/Exonuclease Machine Specific for Protein-DNA Adducts. Mol. Cell *64*, 593–606.

Francia, S., Michelini, F., Saxena, A., Tang, D., de Hoon, M., Anelli, V., Mione, M., Carninci, P., and d'Adda di Fagagna, F. (2012). Site-specific DICER and DROSHA RNA products control the DNA-damage response. Nature *488*, 231–235.

Haber, J.E., Ira, G., Malkova, A., and Sugawara, N. (2004). Repairing a double-strand chromosome break by homologous recombination: revisiting Robin Holliday's model. Philos. Trans. R. Soc. Lond. B Biol. Sci. *359*, 79–86.

Hickson, I.D. (2003). RecQ helicases: caretakers of the genome. Nat. Rev. Cancer *3*, 169–178.

Hu, J., Sun, L., Shen, F., Chen, Y., Hua, Y., Liu, Y., Zhang, M., Hu, Y., Wang, Q., Xu, W., et al. (2012). The intra-S phase checkpoint targets Dna2 to prevent stalled replication forks from reversing. Cell *149*, 1221–1232.

Jasin, M., and Rothstein, R. (2013). Repair of strand breaks by homologous recombination. Cold Spring Harb. Perspect. Biol. *5*, a012740.

Keeney, S., Giroux, C.N., and Kleckner, N. (1997). Meiosis-specific DNA double-strand breaks are catalyzed by Spo11, a member of a widely conserved protein family. Cell *88*, 375–384.

Langerak, P., Mejia-Ramirez, E., Limbo, O., and Russell, P. (2011). Release of Ku and MRN from DNA ends by Mre11 nuclease activity and Ctp1 is required for homologous recombination repair of double-strand breaks. PLoS Genet. *7*, e1002271.

Leland, B.A., Chen, A.C., Zhao, A.Y., Wharton, R.C., and King, M.C. (2018). Rev7 and 53BP1/Crb2 prevent RecQ helicase-dependent hyper-resection of DNA double-strand breaks. eLife *7*, e33402.

Li, L., Germain, D.R., Poon, H.Y., Hildebrandt, M.R., Monckton, E.A., McDonald, D., Hendzel, M.J., and Godbout, R. (2016). DEAD Box 1 Facilitates Removal of RNA and Homologous Recombination at DNA Double-Strand Breaks. Mol. Cell. Biol. *36*, 2794–2810.

Liao, S., Toczylowski, T., and Yan, H. (2008). Identification of the Xenopus DNA2 protein as a major nuclease for the 5′->3′ strand-specific processing of DNA ends. Nucleic Acids Res. *36*, 6091–6100.

Lin, Z., Kong, H., Nei, M., and Ma, H. (2006). Origins and evolution of the recA/RAD51 gene family: evidence for ancient gene duplication and endosymbiotic gene transfer. Proc. Natl. Acad. Sci. USA *103*, 10328–10333.

Marcon, E., and Moens, P.B. (2005). The evolution of meiosis: recruitment and modification of somatic DNA-repair proteins. BioEssays *27*, 795–808.

Mehta, A., and Haber, J.E. (2014). Sources of DNA double-strand breaks and models of recombinational DNA repair. Cold Spring Harb. Perspect. Biol. *6*, a016428.

Michalik, K.M., Böttcher, R., and Förstemann, K. (2012). A small RNA response at DNA ends in Drosophila. Nucleic Acids Res. *40*, 9596–9603.

Michelini, F., Pitchiaya, S., Vitelli, V., Sharma, S., Gioia, U., Pessina, F., Cabrini, M., Wang, Y., Capozzo, I., Iannelli, F., et al. (2017). Damage-induced lncRNAs control the DNA damage response through interaction with DDRNAs at individual double-strand breaks. Nat. Cell Biol. *19*, 1400–1411.

Mimitou, E.P., and Symington, L.S. (2008). Sae2, Exo1 and Sgs1 collaborate in DNA double-strand break processing. Nature *455*, 770–774.

Mimitou, E.P., Yamada, S., and Keeney, S. (2017). A global view of meiotic double-strand break end resection. Science *355*, 40–45.

Nimonkar, A.V., Genschel, J., Kinoshita, E., Polaczek, P., Campbell, J.L., Wyman, C., Modrich, P., and Kowalczykowski, S.C. (2011). BLM-DNA2-RPA-MRN and EXO1-BLM-RPA-MRN constitute two DNA end resection machineries for human DNA break repair. Genes Dev. *25*, 350–362.

Niu, H., Chung, W.H., Zhu, Z., Kwon, Y., Zhao, W., Chi, P., Prakash, R., Seong, C., Liu, D., Lu, L., et al. (2010). Mechanism of the ATP-dependent DNA end-resection machinery from Saccharomyces cerevisiae. Nature *467*, 108–111.

Ohle, C., Tesorero, R., Schermann, G., Dobrev, N., Sinning, I., and Fischer, T. (2016). Transient RNA-DNA Hybrids Are Required for Efficient Double-Strand Break Repair. Cell *167*, 1001–1013.

Orr-Weaver, T.L., and Szostak, J.W. (1983). Yeast recombination: the association between double-strand gap repair and crossing-over. Proc. Natl. Acad. Sci. USA *80*, 4417–4421.

Paull, T.T., and Gellert, M. (1998). The 3′ to 5′ exonuclease activity of Mre 11 facilitates repair of DNA double-strand breaks. Mol. Cell *1*, 969–979.

Persky, N.S., and Lovett, S.T. (2008). Mechanisms of recombination: lessons from E. coli. Crit. Rev. Biochem. Mol. Biol. *43*, 347–370.

Pierce, A.J., Johnson, R.D., Thompson, L.H., and Jasin, M. (1999). XRCC3 promotes homology-directed repair of DNA damage in mammalian cells. Genes Dev. *13*, 2633–2638.

Pierce, A.J., Hu, P., Han, M., Ellis, N., and Jasin, M. (2001). Ku DNA end-binding protein modulates homologous repair of double-strand breaks in mammalian cells. Genes Dev. *15*, 3237–3242.

Plosky, B.S. (2016). The Good and Bad of RNA:DNA Hybrids in Double-Strand Break Repair. Mol. Cell *64*, 643–644.

Przetocka, S., Porro, A., Bolck, H.A., Walker, C., Lezaja, A., Trenner, A., von Aesch, C., Himmels, S.F., D'Andrea, A.D., Ceccaldi, R., et al. (2018). CtIP-Mediated Fork Protection Synergizes with BRCA1 to Suppress Genomic Instability upon DNA Replication Stress. Mol. Cell *72*, 568–582.

Roeder, R.G., Schwartz, L.B., and Sklar, V.E. (1976). Function, structure, and regulation of eukaryotic nuclear RNA polymerases. Symp. Soc. Dev. Biol. *34*, 29–52.

Rothstein, R.J. (1983). One-step gene disruption in yeast. Methods Enzymol. *101*, 202–211.

San Filippo, J., Sung, P., and Klein, H. (2008). Mechanism of eukaryotic homologous recombination. Annu. Rev. Biochem. *77*, 229–257.

Sanjana, N.E., Shalem, O., and Zhang, F. (2014). Improved vectors and genome-wide libraries for CRISPR screening. Nature Methods *11*, 783–784.

Schindelin, J., Arganda-Carreras, I., Frise, E., Kaynig, V., Longair, M., Pietzsch, T., Preibisch, S., Rueden, C., Saalfeld, S., Schmid, B., et al. (2012). Fiji: an open-source platform for biological-image analysis. Nature methods *9*, 676–682.

Schroder, O., Geiduschek, E.P., and Kassavetis, G.A. (2003). A single-stranded promoter for RNA polymerase III. Proc. Natl. Acad. Sci. USA *100*, 934–939.

Seidl, C.I., Lama, L., and Ryan, K. (2013). Circularized synthetic oligodeoxynucleotides serve as promoterless RNA polymerase III templates for small RNA generation in human cells. Nucleic Acids Res. *41*, 2552–2564.

Sturzenegger, A., Burdova, K., Kanagaraj, R., Levikova, M., Pinto, C., Cejka, P., and Janscak, P. (2014). DNA2 cooperates with the WRN and BLM RecQ helicases to mediate long-range DNA end resection in human cells. J. Biol. Chem. *289*, 27314–27326.

Symington, L.S., and Gautier, J. (2011). Double-strand break end resection and repair pathway choice. Annu. Rev. Genet. *45*, 247–271.

Szostak, J.W., Orr-Weaver, T.L., Rothstein, R.J., and Stahl, F.W. (1983). The double-strand-break repair model for recombination. Cell *33*, 25–35.

Thompson, L.H., and Schild, D. (2001). Homologous recombinational repair of DNA ensures mammalian chromosome stability. Mutat. Res. *477*, 131–153.

Wei, H., and Yu, X. (2016). Functions of PARylation in DNA Damage Repair Pathways. Genomics Proteomics Bioinformatics *14*, 131–139.

Wei, W., Ba, Z., Gao, M., Wu, Y., Ma, Y., Amiard, S., White, C.I., Rendtlew Danielsen, J.M., Yang, Y.G., and Qi, Y. (2012). A role for small RNAs in DNA double-strand break repair. Cell *149*, 101–112.

Yan, H., McCane, J., Toczylowski, T., and Chen, C. (2005). Analysis of the Xenopus Werner syndrome protein in DNA double-strand break repair. J. Cell Biol. *171*, 217–227.

Zhang, H., Hua, Y., Li, R., and Kong, D. (2016). Cdc24 Is Essential for Long-range End Resection in the Repair of Double-stranded DNA Breaks. J. Biol. Chem. *291*, 24961–24973.

Zhao, W., Steinfeld, J.B., Liang, F., Chen, X., Maranon, D.G., Jian Ma, C., Kwon, Y., Rao, T., Wang, W., Sheng, C., et al. (2017). BRCA1-BARD1 promotes RAD51-mediated homologous DNA pairing. Nature *550*, 360–365.

Zhou, Y., Caron, P., Legube, G., and Paull, T.T. (2014). Quantitation of DNA double-strand break resection intermediates in human cells. Nucleic Acids Res. *42*, e19.

Zhu, Z., Chung, W.H., Shim, E.Y., Lee, S.E., and Ira, G. (2008). Sgs1 helicase and two nucleases Dna2 and Exo1 resect DNA double-strand break ends. Cell *134*, 981–994.